DOI: 10.15669/pnst.4.341

Progress in Nuclear Science and Technology
Volume 4 (2014) pp. 341-344

ARTICLE

Systematics of thick target neutron yields for reactions of hundred GeV protons on target

Toshiya Sanami[a*], Yosuke Iwamoto[b], Tsuyoshi Kajimoto[c], Nobuhiro Shigyo[d], Masayuki Hagiwara[a], Hee-Seock Lee[e], Erik Ramberg[f], Aria Soha[f], Douglas Jensen[f], Anthony Leveling[f], Nikolai Mokhov[f], David Boehnlein[f], Kamran Vaziri[f], Kenji Ishibashi[d], Yukio Sakamoto[b] and Hiroshi Nakashima[b]

[a]*High Energy Accelerator Research Organization, 1-1 Oho, Tsukuba, Ibaraki 305-0801, Japan;* [b]*Japan Atomic Energy Agency, 2-4 Shirakata, Tokai, Naka, Ibaraki 319-1195, Japan;* [c]*Hiroshima University, Kagamiyama, Higashi-Hiroshima 739-8527, Japan;* [d]*Kyushu University, Motooka, Nishi-ku, Fukuoka 819-0395, Japan;* [e]*Pohang Accelerator Laboratory, POSTECH, Pohang, Kyungbuk 790-784, Republic of Korea;* [f]*Fermi National Accelerator Laboratory, Batavia, IL 60510-5011, USA*

Systematics of neutron energy spectra for 120 GeV protons on C, Al, Cu and W targets are presented for data measured using the time-of-flight technique, room-scattering subtraction, and experimentally determined neutron detection efficiency. The measured neutron energy spectra exhibited low-energy angular-independent and high-energy angular-dependent components, below and above about 50 MeV, respectively. The neutron yields of both components increased linearly with target thickness. We obtained neutron yields for one interaction length target and determine the normalization factors from the ratio of the target thickness to the interaction length. We observed a non-linear relationship between neutron yield and target mass number.

Keywords: neutron yield; angular distribution; target material dependency; 120 GeV protons; NE213 scintillator, time-of-flight; Fermilab test beam line

1. Introduction

Experimental source term-, attenuation-, and activation-data are indispensable for radiation-safety design at high-energy particle accelerator facilities. Ideally, the source term data should include neutron-production rates as well as energy and angular distributions. At present, experimental data are relatively scarce for proton beams above 10 GeV on various targets. Agosteo et al. measured neutron energy and angular distributions for 40 GeV/c mixed proton/pion beams at CERN on several target materials using the Bonner spheres and the unfolding technique [1]. Nakao et al. measured neutron energy spectra for 120 GeV/c mixed proton/pion beams on a copper target behind a concrete and iron shielding wall [2]. The above papers reported systematic discrepancies between experiments and calculations above 10 GeV.

The JASMIN (Japanese American Study for Muon Interaction and Neutron measurement) program was launched in 2007 to measure basic radiation-safety data sets for a 120 GeV proton accelerator facility under well-defined conditions [3-5]: data sets include shielding experiments with activation and the Bonner sphere techniques, induced activities in air and water, and secondary muon interaction and transport. The shielding data showed systematic discrepancies compared with the predictions of multi-particle transport Monte-Carlo codes for both induced activities and neutron spectra.

To study the difference between calculations and experimental data, without uncertainty due to shielding material attenuation and initial guess of the unfolding method, we have measured neutron production as a source term for a 120 GeV proton beam on target. In particular, we have developed a time of flight technique with beam-uniformity correction to measure neutron energy spectra at the Fermilab Test Beam Facility (FTBF) [6]. In this paper, we report neutron energy-spectra systematics (energy, emission angle, target thickness and mass) for 120 GeV protons on C, Al, Cu and W targets using experimental data measured at 15, 30, 45, 90, 120 and 150-degree emission angles [7,8].

2. Methodology

We give only a brief outline of the neutron-measurement methodology and data taking procedures: more detail can be found in references [6,7,8].

The main features of this experiment are: (1) neutron-energy determination using the time-of-flight (TOF) technique, (2) use of experimental neutron detection efficiency [9], (3) experimental subtraction of room-scattered neutron effects, and (4) direct counting

*Corresponding author. Email: toshiya.sanami@kek.jp

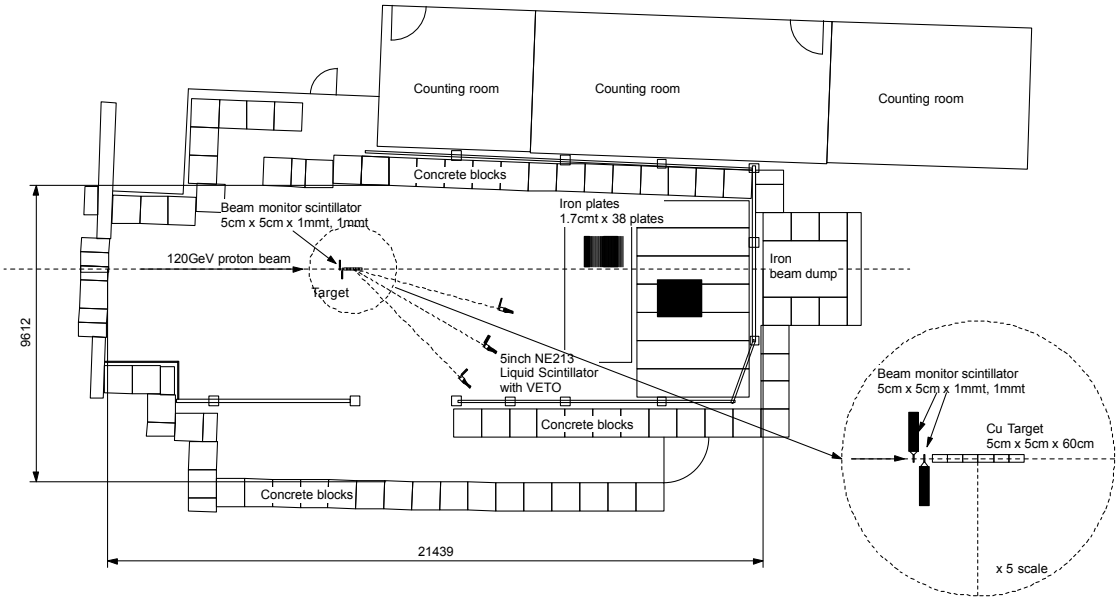

Figure 1. Experimental arrangement for neutron measurements at the FTBF.

of primary protons. Feature (1) permits precise determination of neutron energy. Features (2) and (4) provide reliable absolute normalization, whereas feature (3) allows for direct comparison between experimental results and theoretical calculations.

Figure 1 shows the experimental arrangement in the MT6-2 experimental area of the FTBF. We placed the neutron production target on the beam line near the center of the MT6-2 room, and enclosed the area with an assembly of 0.9 m(W) 0.9 m(D) 2.7 m(H) concrete blocks. The area has no roof. A 120 GeV proton beam with 3×10^5 protons/spill was transported to the target area, and two plastic scintillators were placed in front of the target to count the number of protons. We used a wire chamber readout to maintain the beam position at the target center and to keep the beam size to 5 mm diameter of full-width at half maximum (FWHM).

An NE213 liquid scintillator (diameter 12.7-cm, length 12.7 cm), coupled with a photo multiplier tube, was used to measure neutron production at the target. We used a thin plastic scintillator placed in front of the NE213 scintillator to discard charged particle events. Depending on the measured angles, distances from the center of the target to the front face of the NE213 scintillator ranged from 4 to 7 m.

Table 1. Targets with corresponding dimensions, densities, hadron interaction lengths (λ_I), and emission angles.

	A	Length	Radius	Density	λ_I	Measured angle			
		cm	cm	g/cm^3	cm	30	45	120	150
Graphite	12	60	2.5	1.81	47.4	✓	✓	-	-
Aluminum	27	50	1.75	2.7	39.7	✓	✓	✓	✓
Copper	63	20	2.82 (5×5)	8.96	15.3	✓	✓	✓	✓
		40			15.3	✓	✓	✓	✓
		60			15.3	✓	✓	-	-
Tungsten	184	10	1.5	18.1	10.6	✓	✓	✓	✓

We used two systems, namely a waveform data taking 10-bit fast digitizer (Agilent Acqiris DC282) and a combination of standard NIM-CAMAC modules to process detector signals [7,8]. We analyzed results mainly from the latter system, since the former exhibited relatively large uncertainties at forward angles: the floor scattering components increase with decreasing angle because of the forward peaked angular distribution of secondary neutrons and longer flight paths.

Table 1 lists the targets with dimensions, densities, hadron interaction lengths (λ_I), and emission angles for data taken with the standard NIM-CAMAC module system.

For each target, we performed two data taking runs, with and without an iron shadow bar of 12-cm square and 1.0-m length. We placed the shadow bar on the pathway from the target to the detector to measure only room-scattered neutrons. Typical target run times ranged from 4 to 8 hours [7].

We used the following equation to extract the neutron energy spectrum ($d^2Y(E)/dEd\Omega$) from raw data at each emission angle [6,8]:

$$\frac{d^2Y(E)}{dEd\Omega} = \frac{1}{\varepsilon(E)\cdot\Delta E\cdot S}\left[\left(\frac{C_n(E)f_{dead}}{N_p f_{tof} f_{multi}}\right)_{out} - \left(\frac{C_n(E)f_{dead}}{N_p f_{tof} f_{multi}}\right)_{in}\right], \quad (1)$$

where the subscripts, *out* and *in*, denote measurements without and with the shadow bar, respectively. $C_n(E)$ refers to the neutron count per energy bin after n-γ and charged particle discrimination, N_p denotes the number of protons, $\varepsilon(E)$ specifies neutron detection efficiency of the NE213 determined experimentally at LANSCE, LANL [9], S represents the detector surface area, and ΔE denotes the energy spectrum bin width. There are three correction factors in Eq. (1), namely: f_{dead} corrects for

uncountable events due to data acquisition system dead time; f_{tof} corrects for TOF event loss associated with multiple proton beam events for single neutron detection; and f_{multi} corrects for N_p count loss due to pulse pileup.

3. Results and discussion

3.1. Neutron energy spectra

Figure 2 shows neutron energy spectra from 25 MeV to 3000 MeV at 30, 45, 120, and 150-degree emission angles for a 40-cm-long copper target. The neutron spectra consist of two components, below and above 50 MeV. The high-energy component above 50 MeV, exhibits a strong angular dependency, whereas the low-energy component below 50 MeV is almost independent of the emission angle. We observe similar trends for the neutron spectra of the other targets.

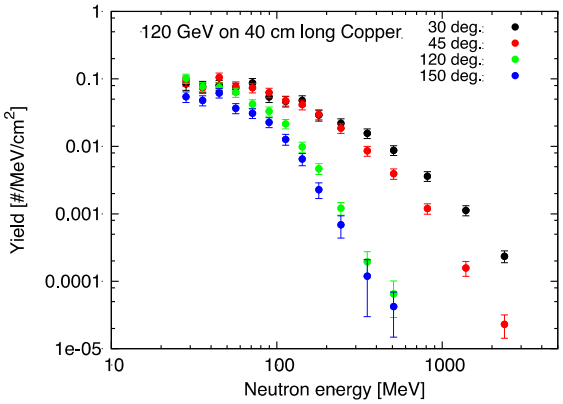

Figure 2. Neutron energy spectra at 30, 45, 120, and 150 degrees emission angles for a 40-cm-long copper target.

3.2. Neutron yield angular distributions

Next, we compute integral yields below and above 50 MeV to study distribution systematics.

Figure 3 shows neutron yields for low- and high-energy components as a function of emission angle. The two components show different angular dependence: the low-energy component exhibits an almost flat angular distribution, whereas the high-energy component increases rapidly with decreasing emission angle. The lines in Figure 3 correspond to least-square fitting using linear and exponential equations for the low- and high-energy components, respectively. The fitting lines intersect at about 180 degrees, meaning that the component yields are comparable at this angle. The data for the other targets show similar trends. Although the number of data points is insufficient to deduce an empirical formula, the above trends could be useful for determining neutron yield systematics as well as validating simulation results.

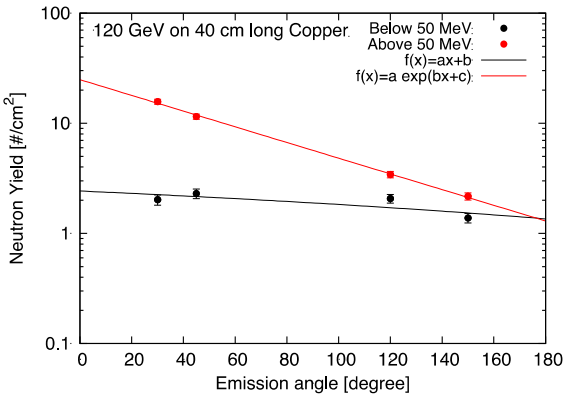

Figure 3. Neutron-yield angular distributions of low- and high-energy components for a 40-cm-long copper target.

3.3. Neutron yields as a function of target thickness

Figure 4 shows low- and high- energy component neutron-yields at a 45-degree emission angle for a copper target as a function of target thickness in hadron interaction length (λ_I) units: we only considered three different target thicknesses for the copper target. We used a linear function to obtain least square fits of the experimental neutron yields. Both components saturate at around three to four λ_I, but increase linearly with target thickness up to a few λ_I, meaning that neutrons from external nuclear cascade processes are not dominant. We normalized the yield to a target thickness of 1 λ_I, assuming that the yield increases linearly. Because the other target thicknesses were less than a few λ_I, the normalization allows us to compare neutron yields for different target materials.

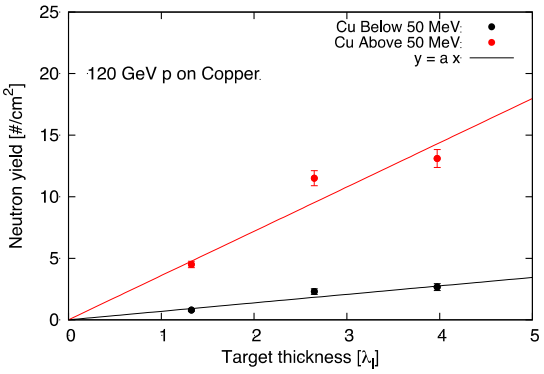

Figure 4. Neutron-yields for low- and high-energy components at a 45 degrees emission angle as a function of target thickness in interaction length (λ_I) units for a copper target.

3.4. Target material dependency

Figure 5 shows neutron yields normalized to 1 λ_I of the target thickness for low- and high- energy components as a function of target mass number. Although the number of data points is limited, we observe the following non-linear increase of yield with

target mass number:

$$Y = a\left(1-\exp(-x/b)\right), \tag{2}$$

where Y denotes neutron yield, x is mass number, and a and b represent fitting parameters.

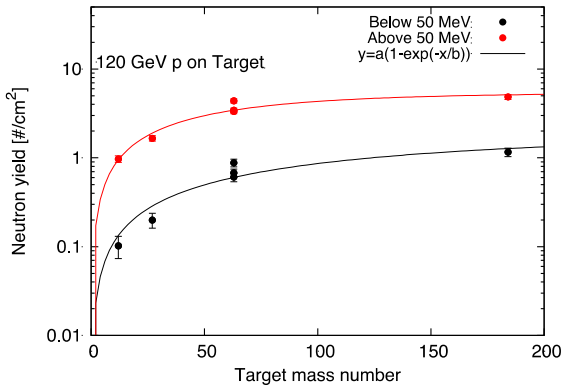

Figure 5. Neutron yields for low- and high-energy components at a 45 degrees emission angle as a function of target mass number.

4. Conclusion

We studied neutron energy-spectra systematics for 120 GeV proton beams on C, Al, Cu and W targets for low- and high-energy components as a function of neutron emission angle, target thickness, and target mass number. Although we obtained only a few data points, these systematics will be useful for verifying calculations and other experimental data. Future studies will focus on neutron yield as a function of incident energy.

Acknowledgement

This work was supported by a grand-aid from the Ministry of Education, Culture, Sports, Science and Technology (KAKENHI 19360432 and 21360473) in Japan.

References

[1] S. Agosteo, C. Birattari, E. Dimovasili, A. Foglio Para, M. Silari, L. Ulrici and H. Vincke, *Nucl. Instrum. Meth.* B 229 (2005), pp. 24–34.

[2] N. Nakao, S. Taniguchi, S. Roesler, M. Brugger, M. Hagiwara, H. Vincke, H. Khater, A.A. Prinz, S.H. Rokni and K. Kosako, *Nucl. Instrum. Meth.* B 266 (2008), pp.93– 106.

[3] H. Nakashima, N.V. Mokhov, A. Leveling, D. Boehnlein, N.Nakao, K. Vaziri, V. Cupps, B. Kershisnik, S. Benesch, G. Lautenschlager, J. Leo, W. Schmitt, B. Arnord, A.Elste, D. Hicks, J. Chyllo, C. James, M. Andrews, J. Hylen, K. Graden, N. Grossman, K. Schuh, Y. Kasugai, N. Matsuda, Y. Iwamoto, Y. Sakamoto, A.F. Leveling, D.J. Boehnlein, K. Vaziri, T. Sanami, H. Matsumura, H. Iwase, M. Hagiwara, A. Toyoda, S. Ban, H. Hirayama, K. Oishi, T. Nakamura, N. Shigyo, H. Arakawa, T. Kajimoto, K. Ishibashi, H Yashima, S. Sekimoto, N. Kinoshita, H. S. Lee and K. Niita, JASMIN: Japanese- American study of muon interactions and neutron detection, *Proceedings of 10th Workshop of Shielding Aspects of Accelerators, Targets and irradiation facilities,* CERN, Switzerland, 2–4 June (2010), pp. 235.

[4] Y. Kasugai, N. Matsuda, Y. Iwamoto, Y. Sakamoto, H. Nakashima, H. Matsumura, N. Kinoshita, H. Iwase, T. Sanami, M. Hagiwara, H. Hirayama, H. Yashima, N. Sigyo, H.Arakawa, K. Ishibashi, N.V. Mokhov, A. Leveling, D. Boehnlein, K. Vazili, G. Lauten, S. Wayne, V. Cupps, B. Kershisnik, S. enesch, T. Nakamura, K. Oishi and K. Niita, Shielding experiments under JASMIN collaboration at FERMILAB (I) overview of the research activities, *J. Korean Phys. Soc.* 59 (2) (2011), pp.2063–2066.

[5] M. Hagiwara, T. Sanami, Y. Iwamoto, H. Arakawa, N. Shigyo, N.V. Mokhov, A.F. Leveling, D.J. Boehnlein, K. Vaziri, T. Nakamura, K. Oishi, H. Hirayama, H. Nakashima, Y. Sakamoto and members of JASMIN collaboration, Shielding experiments at high energy accelerators of fermilab (III): neutron spectrum measurements in intense pulsed neutron fields of the 120-GeV proton facility using a current bonner sphere technique, *Prog. Nucl. Sci. Technol.* 1 (2011), pp.52–56.

[6] T. Sanami, Y. Iwamoto, T. Kajimoto, N. Shigyo, M. Hagiwara, H.S. Lee, E. Ramberg, R. Coleman, A. Soha, D. Jensen, A. Leveling, N.V. Mokhov, D. Boehnlein, K. Vaziri, K. Ishibashi, Y. Sakamoto and H. Nakashima, *Nucl. Instrum. Meth.* B 274 (2012), pp.26–35.

[7] T. Kajimoto, Doctor thesis of Kyushu University (2012) [in Japanese].

[8] Y. Iwamoto, T. Sanami, T. Kajimoto, N. Shigyo, M. Hagiwara, H.S. Lee, E. Ramberg, R. Coleman, A. Soha, D. Jensen, A. Leveling, N.V. Mokhov, D. Boehnlein, K. Vaziri, K. Ishibashi, Y. Sakamoto and H. Nakashima, *Proceedings of ISORD6*, in print.

[9] T. Kajimoto, N. Shigyo, T. Sanami, K. Ishibashi, R. C. Haight and N. Fotiades, *Nucl. Instr. and Meth.* A 665 (2011), pp.80.